JACS
JOURNAL OF THE AMERICAN CHEMICAL SOCIETY

Communication

pubs.acs.org/JACS

Mechanism of the Formation of a Mn-Based CO_2 Reduction Catalyst Revealed by Pulse Radiolysis with Time-Resolved Infrared Detection

David C. Grills,* Jaime A. Farrington,† Bobby H. Layne, Sergei V. Lymar, Barbara A. Mello, Jack M. Preses, and James F. Wishart

Chemistry Department, Brookhaven National Laboratory, P.O. Box 5000, Upton, New York 11973-5000, United States

Supporting Information

ABSTRACT: Using a new technique, which combines pulse radiolysis with nanosecond time-resolved infrared (TRIR) spectroscopy in the condensed phase, we have conducted a detailed kinetic and mechanistic investigation of the formation of a Mn-based CO_2 reduction electrocatalyst, $[Mn(^tBu_2\text{-bpy})(CO)_3]_2$ ($^tBu_2$-bpy = 4,4′-$^tBu_2$-2,2′-bipyridine), in acetonitrile. The use of TRIR allowed, for the first time, direct observation of all the intermediates involved in this process. Addition of excess $[^nBu_4N][HCO_2]$ to an acetonitrile solution of *fac*-$MnBr(^tBu_2\text{-bpy})(CO)_3$ results in its quantitative conversion to the Mn−formate complex, *fac*-$Mn(OCHO)(^tBu_2\text{-bpy})(CO)_3$, which is a precatalyst for the electrocatalytic reduction of CO_2. Formation of the catalyst is initiated by one-electron reduction of the Mn−formate precatalyst, which produces the bpy ligand-based radical. This radical undergoes extremely rapid (τ = 77 ns) formate dissociation accompanied by a free valence shift to yield the five-coordinate Mn-based radical, $Mn^{\bullet}(^tBu_2\text{-bpy})(CO)_3$. TRIR data also provide evidence that the Mn-centered radical does not bind acetonitrile prior to its dimerization. This reaction occurs with a characteristically high radical−radical recombination rate ($2k_{dim} = (1.3 \pm 0.1) \times 10^9$ M^{-1} s^{-1}), generating the catalytically active Mn−Mn bound dimer.

Recent work[1] has shown that the manganese complexes, *fac*-$MnBr(R_2\text{-bpy})(CO)_3$ (**1**; R_2-bpy = 4,4′-R_2-2,2′-bipyridine; R = H, Me, or ^{t}Bu), which are analogues of a well-established family of rhenium catalysts,[2] can act as precatalysts for the efficient and selective electrocatalytic reduction of CO_2 to CO in acetonitrile (CH_3CN) in the presence of Brønsted acids. The Mn-based catalysts are of considerable interest because they contain an earth-abundant first-row transition metal and facilitate CO_2 reduction at ∼0.3 V lower overpotential than their Re counterparts, while exhibiting a similar catalytic activity (particularly for R = ^{t}Bu).[1b] The proposed mechanism[1a,b] begins with formation of the active catalytic species **4** and **5** from the precatalyst **1** as shown in eqs 1−4 (see Chart S1 for chemical structures).

Once formed, species **4** and **5** engage in the catalytic cycle by two pathways: (i) a two-electron pathway in which **5** is the catalytically active species that reacts with CO_2,[1] and (ii) a one-electron pathway in which the Mn−Mn bound dimer **4** is reactive toward CO_2 and H^+, forming a Mn(II) hydroxycarbonyl intermediate, *mer*-$[Mn(Me_2\text{-bpy})(CO)_3(C(O)OH)]^+$ that was identified by pulsed EPR.[1c] A very recent paper[3] also describes the use of **1** (R = H) as a precatalyst for the reduction of CO_2 to formic acid in a photocatalytic system that makes use of $[Ru(Me_2\text{-bpy})_3]^{2+}$ as a visible light-absorbing photosensitizer and 1-benzyl-1,4-dihydronicotinamide (BNAH) as a sacrificial electron donor. In that case, formation of dimer **4** was initially observed, followed by its decay upon further irradiation into an as yet unidentified "Mn species" that is presumed to be the active catalyst.

$$MnBr(R_2\text{-bpy})(CO)_3(\mathbf{1}) + e^- \rightarrow [MnBr(R_2\text{-bpy}^{\bullet -})(CO)_3]^-(\mathbf{2}) \quad (1)$$

$$\mathbf{2} \rightarrow Mn^{\bullet}(R_2\text{-bpy})(CO)_3(\mathbf{3}) + Br^- \quad (2)$$

$$\mathbf{3} + \mathbf{3} \xrightarrow{k_{dim}} (CO)_3(R_2\text{-bpy})Mn\text{-}Mn(R_2\text{-bpy})(CO)_3(\mathbf{4}) \quad (3)$$

$$\mathbf{4} + 2e^- \rightarrow 2[Mn(R_2\text{-bpy})(CO)_3]^-(\mathbf{5}) \quad (4)$$

Clearly, there is still much to learn about the mechanism of CO_2 reduction catalysis with Mn complexes, and gaining this knowledge is of critical importance in terms of developing a new generation of low-cost catalysts that are suitable for practical applications. The techniques applied so far have revealed important information, but they have not allowed some of the intermediate species to be observed, e.g., **2**, **3**, and any CO_2 adducts other than the hydroxycarbonyl species measured at low temperature by EPR.[1c] We have begun to address these issues by making use of pulse radiolysis combined with nanosecond-TRIR detection, focusing initially on the one-electron reduction of a new Mn−formate complex, *fac*-$Mn(OCHO)(^tBu_2\text{-bpy})(CO)_3$ (**6**), and its subsequent conversion to the dinuclear catalyst **4** (eqs 9, 10, and 3). Cyclic voltammetry measurements have shown that **6** is indeed an effective precatalyst for electrocatalytic CO_2 reduction, behaving identically to **1** (see Figure S3).

Pulse radiolysis utilizes a short, high-energy electron pulse for the rapid production of radical ions.[4] The subsequent reactions of these species are typically monitored by transient absorption (TA) spectroscopy in the UV/vis/near-IR regions. However, the often-broad absorption bands can make the identification of reactive intermediates challenging. To overcome this limitation, researchers have turned to TRIR detection, which takes

Received: January 30, 2014
Published: March 28, 2014

   dx.doi.org/10.1021/ja501051s | J. Am. Chem. Soc. 2014, 136, 5563−5566

advantage of the structural specificity of mid-IR spectroscopy. However, until we recently developed a nanosecond TRIR detection capability for condensed-phase pulse radiolysis,[5] this had been restricted to a handful of gas-phase studies on the microsecond time scale[6a,b] and an FTIR-based approach with ~30 s time resolution.[7] Laser flash photolysis combined with TRIR detection is a well-established alternative approach for the investigation of transient intermediates.[8] However, it is not applicable to the chemistry under investigation here due to the extreme photosensitivity of **1** that results in CO ligand loss and/or light-induced isomerization.[9]

Pulse radiolysis of CH_3CN results in the formation of solvated electrons, e_s^-, solvent radicals, $^\bullet CH_2CN$, and protons (eq 5).[10] Since e_s^- is a strong reducing agent, rapid one-electron reduction of a dissolved solute ensues.[10a,c] In the presence of formate anion, it has been shown that the oxidizing side product, $^\bullet CH_2CN$ can be scavenged via hydrogen atom transfer, resulting in the production of a second reducing equivalent, $CO_2^{\bullet-}$, as shown in eq 6.[11] In principle, this should result in a net doubling of the yield of the one-electron reduced (OER) solute (eq 7). Further details of these processes are provided in the SI.

$$CH_3CN \rightsquigarrow e_s^-,\ ^\bullet CH_2CN,\ H^+ \quad (5)$$

$$^\bullet CH_2CN + HCO_2^- \rightarrow {}^\bullet CH_3CN + CO_2^{\bullet-} \quad (6)$$

$$2\ \text{solute} + e_s^-,\ CO_2^{\bullet-} \rightarrow 2\ \text{solute}^{\bullet-} + CO_2 \quad (7)$$

Since it is essential to eliminate $^\bullet CH_2CN$ from the reaction mixture, all of our pulse radiolysis measurements were performed in the presence of 50 mM formate. IR and NMR spectroscopy revealed that under these conditions, the bromide ligand of **1** is quantitatively displaced by formate in the time of mixing, to generate the formate complex **6** (eq 8, see SI for IR and NMR spectra). Previous IR spectroelectrochemical (SEC) measurements on **1** (and its chloride analogue) have shown that one-electron reduction results in dimer **4** as the only observed product.[1b,12] It was assumed that the OER species, **2**, is unstable, rapidly losing Br^- (or Cl^-), followed by the resulting radicals dimerizing within the time scale of the electrochemical experiment. In this work, we are investigating the analogous conversion of **6** to **4** (eqs 9, 10, and 3). Since **7** and **3** have never been experimentally observed, we used density functional theory (DFT)[13] to calculate the ν(CO) IR spectra of all the Mn species in eqs 9, 10, and 3 (**6**, **7**, **3** and **4**; R = ^{t}Bu), together with another possible intermediate that may result from the reaction of **3** with CH_3CN, i.e., the ligand-localized radical, *fac*-Mn(^{t}Bu$_2$-bpy$^{\bullet-}$)-(CO)$_3$(CH$_3$CN) (**8**). These DFT-calculated spectra will provide a useful comparison with the pulse radiolysis-TRIR spectra and are shown in Figure 1, with the band positions listed in Table S1.

$$\text{MnBr}(^t\text{Bu}_2\text{-bpy})(\text{CO})_3(\mathbf{1}) + HCO_2^- \xrightarrow{-Br^-} \text{Mn(OCHO)}(^t\text{Bu}_2\text{-bpy})(\text{CO})_3(\mathbf{6}) \quad (8)$$

$$\mathbf{6} + e^- \xrightarrow{k_e} [\text{Mn(OCHO)}(^t\text{Bu}_2\text{-bpy}^{\bullet-})(\text{CO})_3]^-(\mathbf{7}) \quad (9)$$

$$\mathbf{7} \xrightarrow{k_{dis}} \text{Mn}^\bullet(^t\text{Bu}_2\text{-bpy})(\text{CO})_3(\mathbf{3}) + HCO_2^- \quad (10)$$

In Figure 1, we see that the initial OER product, **7**, should exhibit an ~25 cm^{-1} red-shift of its ν(CO) bands relative to **6**. Like **6**, **7** is a Mn(I) species, but it is negatively charged with the extra electron residing largely in the π^* orbitals of the bpy ligand. Due to orbital overlap, this results in additional electron density

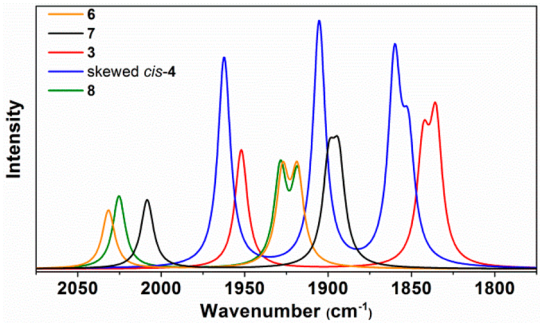

Figure 1. DFT-calculated IR spectra (9 cm^{-1} Gaussian fwhm) of species **3**–**4** (R = ^{t}Bu) and **6**–**8**, calculated with a conductor polarizable continuum model for CH_3CN.

on the Mn center and increased π back-bonding into the π^*(CO) antibonding orbitals, resulting in a weakening of the CO bonds. The five-coordinate radical **3** has three ν(CO) bands that are shifted further to the red relative to those of **7**, since **3** is a Mn(0) species with the unpaired electron residing mainly on the metal center. The calculated IR spectrum of the skewed *cis* isomer[14] of **4** is in good agreement with experiment.[1b] The solvent-bound, ligand-localized radical **8** will have ν(CO) IR bands that are very close to those of **6**, since it is a neutral Mn(I) species. The locations of the unpaired electrons in **7**, **3** and **8** can be seen in their calculated singly occupied molecular orbitals (SOMO's) in Figure S1.

TRIR spectra at three selected time delays after pulse radiolysis of a solution of **6** in CH_3CN are shown in Figure 2. All ν(CO) IR

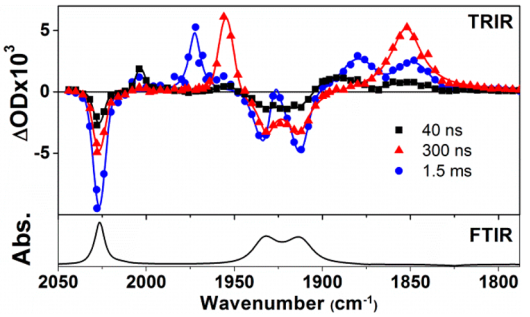

Figure 2. IR spectrum of a 1.5 mM solution of **6** in CH_3CN containing 50 mM [^{n}Bu$_4$N][HCO$_2$] (bottom) and TRIR spectra recorded 40 ns,[15] 300 ns, and 1.5 ms after pulse radiolysis of this argon-purged solution (top). The black, red, and blue spectra correspond to completion of the reactions in eqs 9, 10, and 3, respectively.

band positions of the observed transient species are listed in Table S1. At 40 ns (black spectrum, shown in more detail in Figure S4), bleaching of the ν(CO) bands of **6** is observed, together with two new transient bands at 2004 and 1892 cm^{-1}.[15] The lower frequency band is broad and likely an overlap of two bands. These transient bands decay exponentially ($\tau \approx 60$ ns, see Figure S8) to reveal a new pair of ν(CO) bands at 1955 and 1853 cm^{-1} (red spectrum). Again, the lower frequency band is broad and likely results from the overlap of two bands. Finally, these two ν(CO) bands disappear through second-order kinetics on the millisecond time scale (Figure 3) to yield four new ν(CO) bands at 1973, 1927, 1880, and 1849 cm^{-1} (blue spectrum), which correspond to the dimer **4**.[1b]

Although the 1927 cm^{-1} band of **4** in the TRIR spectrum at 1.5 ms is obscured by the broad bleach bands in this region, it is

dx.doi.org/10.1021/ja501051s | J. Am. Chem. Soc. 2014, 136, 5563–5566

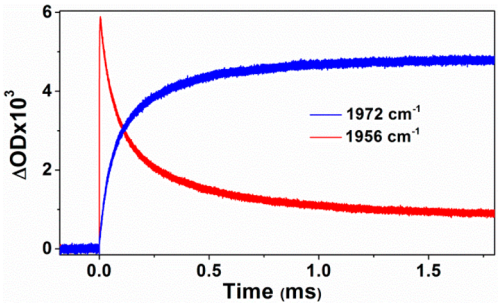

Figure 3. TRIR kinetic traces recorded after pulse radiolysis of an argon-purged 1.5 mM solution of **6** in CH_3CN containing 50 mM [^{n}Bu$_4$N][HCO_2] at 1956 cm^{-1} (red) and 1972 cm^{-1} (blue).

evident from the way it diminishes the bleach intensity at this frequency compared to the other time delays. Note that the gradually increasing bleach intensity between the successive TRIR spectra is explained by the ~40 ns response time of the TRIR apparatus (black to red spectra, see also Figure S8) and the reduction of a second equivalent of **6**, presumably by $CO_2^{\bullet-}$ (red to blue spectra, eqs 6 and 7 and Figure S7).

The 2004 and 1892 cm^{-1} bands observed immediately after pulse radiolysis were confirmed to be due to a Mn carbonyl species by a control experiment in the absence of **6**, in which no significant transient signals were observed. We can confidently assign these bands to the OER species, **7**, by comparison with the DFT-calculated spectrum of **7** (Figure 1 and Table S1) and a pulse radiolysis experiment on the related *fac*-ReBr(^{t}Bu$_2$-bpy)(CO)$_3$ complex **9** (Figure S5). The next transient observed (ν(CO) at 1955 and 1853 cm^{-1}) is assigned as a neutral radical species resulting from formate dissociation from **7**. The positions of the ν(CO) bands of this radical provide useful information about the Mn coordination environment. They are an average of 44 cm^{-1} lower in frequency than those of **7** and are a close match to the DFT-calculated IR bands of the metal-based radical **3**. In contrast, the calculated bands of the solvent-bound ligand-localized radical **8** lie at much higher frequencies (Figure 1 and Table S1), which indicates that the species generated upon formate dissociation from **7** exists as the five-coordinate metal-based radical **3**, with no binding of a solvent molecule occurring at the vacant coordination site. This conclusion agrees with previous IR-SEC observations on the Re analogue, Re$^{\bullet}$(^{t}Bu$_2$-bpy)(CO)$_3$,[16] that was shown to exist as a five-coordinate radical in CH_3CN. Interestingly, previous data on related [Re(α-diimine)(CO)$_3$L]$^{n+}$ and [Re(α-diimine)(CO)$_3$]$_2$ complexes have indicated that in coordinating solvents, such as CH_3CN, the neutral radical generated after dissociation of L from the OER species or by homolysis of the Re–Re bond exists as a six-coordinate solvent complex with the unpaired electron being shifted from the metal to the α-diimine ligand.[17] Thus, the two ^{t}Bu substituents on the bpy ligand in **3** must have sufficient electron donating ability to destabilize such a complex and favor the five-coordinate metal-based radical, as was previously suggested for the Re analogue.[16] Although we should expect the radical–radical reaction between $CO_2^{\bullet-}$ and **3** to form a CO_2 adduct, i.e., *fac*-[Mn(^{t}Bu$_2$-bpy)(CO)$_3$(CO_2)]$^-$ (**11**) in the pulse radiolysis experiments, it can be shown that this reaction does not significantly interfere with the dimerization of **3** via reaction 3 (see SI).

To more accurately measure the rate of formate dissociation from **7**, we have performed a complementary pulse radiolysis experiment with vis/near-IR TA detection, since the TA apparatus has a much faster response time than the TRIR system (~1.5 vs ~40 ns). TA spectra measured after pulse radiolysis are shown in Figure 4. Immediately after the electron

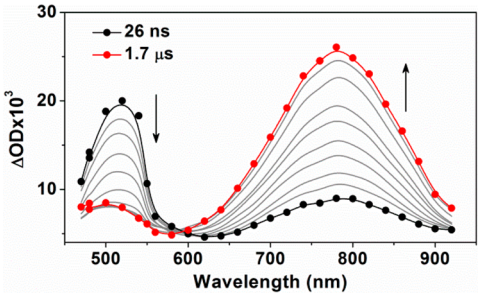

Figure 4. TA spectra recorded after pulse radiolysis of a 3.0 mM solution of **6** in argon-purged CH_3CN containing 50 mM [^{n}Bu$_4$N][HCO_2].

pulse, TA bands are observed at 520 and 790 nm. These are assigned to **7**, based on a comparison with the known spectrum[18] of *fac*-[ReCl(bpy$^{\bullet-}$)(CO)$_3$]$^-$ and our TD-DFT calculated spectrum of **7** (Figure S9). With time, these bands are replaced by an intense absorption at 780 nm and a weaker band at ~500 nm. These are assigned to **3**, again based on a comparison with the TD-DFT calculated spectrum of **3** (Figure S9). Exponential fits of kinetic traces at different wavelengths yielded a rate constant for formate dissociation from **7** of $k_{dis} = 1.3 \times 10^7$ s^{-1} (Figure S11).

The time scale for formate dissociation from **7** (τ = 77 ns) is significantly shorter than that of bromide dissociation from the Re–Br analogue, *fac*-[ReBr(^{t}Bu$_2$-bpy$^{\bullet-}$)(CO)$_3$]$^-$ (**10**) by at least 7 orders of magnitude (see Figure S5). The short lifetime of **7** parallels previous observations by IR-SEC on **1**, in which **2** and **3** could not be observed upon one-electron reduction of **1** to generate dimer **4**, due to the instability and short lifetime of **2**.[1b,12] The labilization of the halide ligand in reduced [MX(α-diimine$^{\bullet-}$)(CO)$_3$]$^-$ complexes (M = Mn or Re) results from an overlap of the partially filled α-diimine π^* orbital with the σ^*(M–X) antibonding orbital.[19] Presumably, a similar effect is occurring in the reduced Mn–formate complex **7**, with charge leakage into the Mn center being more efficient than in the OER Re–Br complex **10** due to better matching of the Mn 3d orbitals with the α-diimine π^* orbital.[20]

The magnitude of the rate constant for dimerization of **3** to **4** (k_{dim}, eq 3) provides further insight into the nature of the Mn coordination environment in **3**. To determine k_{dim}, we took advantage of the well-separated ν(CO) IR bands of **6**, **3**, and **4** and measured the TRIR decay kinetics of **3** as a function of its initial concentration; the latter was modulated through changing the per pulse radiation dose (see Figures S12 and S13 and discussion). From these experiments, the dimerization rate constant was determined to be $2k_{dim} = (1.3 \pm 0.1) \times 10^9$ M^{-1} s^{-1}. This value is some orders of magnitude greater than typical dimerization rate constants observed for solvent-coordinated metal complexes with ligand-localized radicals; for instance, $2k$ = 40 M^{-1} s^{-1} has been reported for dimerization of Re(Me$_2$-bpy$^{\bullet-}$)(CO)$_3$(THF) in THF.[17b] Although the k_{dim} value that we have determined for the Mn-based radical is somewhat below the diffusion-controlled limit of ~10^{10} M^{-1} s^{-1}, this deviation can be explained by the below unity steric factor. Indeed, only a fraction of radical–radical encounters can result in dimerization due to the screening of the Mn-centered free valence by the surrounding ligands. We thus take the high k_{dim} value as evidence that the Mn-

dx.doi.org/10.1021/ja501051s | J. Am. Chem. Soc. 2014, 136, 5563–5566

centered radical does not bind CH_3CN prior to its dimerization and is best formulated as *fac*-Mn$^{\bullet}$(^{t}Bu$_2$-bpy)(CO)$_3$.

In conclusion, we have used the newly developed technique of condensed-phase pulse radiolysis combined with TRIR spectroscopy, together with conventional TA detection, to examine the mechanistic details of the formation of a Mn-based CO_2 reduction electrocatalyst, [Mn(^{t}Bu$_2$-bpy)(CO)$_3$]$_2$, upon one-electron reduction of a new precatalyst, *fac*-Mn(OCHO)(^{t}Bu$_2$-bpy)(CO)$_3$ in CH_3CN. This precatalyst is generated by dissolution of the previously investigated[1b] precatalyst, *fac*-MnBr(^{t}Bu$_2$-bpy)(CO)$_3$ in CH_3CN in the presence of excess formate, which is used for scavenging the radiolytically generated solvent radical. The use of TRIR detection allowed, for the first time, the direct observation and identification of all the intermediates in the catalyst formation process. The reduced precatalyst is a bpy ligand-based radical, which undergoes rapid (τ = 77 ns) formate dissociation to yield a five-coordinate Mn-based radical, *fac*-Mn$^{\bullet}$(^{t}Bu$_2$-bpy)(CO)$_3$. The Mn-based radicals dimerize with a characteristically high radical−radical recombination rate ($2k_{dim} = (1.3 \pm 0.1) \times 10^9$ M^{-1} s^{-1}), providing further evidence that they exist as five-coordinate species in CH_3CN. Future work will focus on the next stage of the catalytic cycle that involves the reduction of the Mn−Mn dimer and its subsequent reactions with CO_2, in the presence and absence of Brønsted acids. Since these processes could involve the formation of formate-like adducts, it may become necessary to replace formate by a potentially less interfering solvent radical scavenger for these studies (details in SI).

It is clear that the combination of pulse radiolysis and TRIR spectroscopy is a powerful and useful technique for the rapid production, identification, and kinetic monitoring of short-lived intermediates that are involved in redox catalysis. We believe this method will play an increasing role in unraveling the mechanisms of such processes, thus contributing to the development of new generations of catalysts.

■ ASSOCIATED CONTENT

Supporting Information

Experimental details, characterization data, and complete ref 13. This material is available free of charge via the Internet at http://pubs.acs.org.

■ AUTHOR INFORMATION

Corresponding Author

dcgrills@bnl.gov

Present Address

[†]Sydor Instruments LLC, 291 Millstead Way, Rochester, NY.

Notes

The authors declare no competing financial interest.

■ ACKNOWLEDGMENTS

This work, and use of the LEAF Facility of the BNL Accelerator Center for Energy Research, was supported by the US Department of Energy (DOE), Office of Basic Energy Sciences, Division of Chemical Sciences, Geosciences & Biosciences under contract no. DE-AC02-98CH10886 and by BNL Program Development funding. B.A.M. thanks the DOE and BNL's Office of Educational Programs for a SULI internship. We are also grateful to the DOE for FY2010 supplemental capital funding. We thank Drs. Etsuko Fujita and Jim Muckerman for helpful discussions.

■ REFERENCES

(1) (a) Bourrez, M.; Molton, F.; Chardon-Noblat, S.; Deronzier, A. *Angew. Chem., Int. Ed.* **2011**, *50*, 9903. (b) Smieja, J. M.; Sampson, M. D.; Grice, K. A.; Benson, E. E.; Froehlich, J. D.; Kubiak, C. P. *Inorg. Chem.* **2013**, *52*, 2484. (c) Bourrez, M.; Orio, M.; Molton, F.; Vezin, H.; Duboc, C.; Deronzier, A.; Chardon-Noblat, S. *Angew. Chem., Int. Ed.* **2013**, *53*, 240.

(2) Hawecker, J.; Lehn, J. M.; Ziessel, R. *Helv. Chim. Acta* **1986**, *69*, 1990.

(3) Takeda, H.; Koizumi, H.; Okamoto, K.; Ishitani, O. *Chem. Commun.* **2014**, *50*, 1491.

(4) (a) Tabata, Y. *Pulse Radiolysis*; CRC Press: Boca Raton, FL, 1990. (b) *Recent Trends in Radiation Chemistry*; Wishart, J. F., Rao, B. S. M., Eds.; World Scientific Publishing Co.: Singapore, 2010.

(5) Grills, D. C.; Cook, A. R.; Fujita, E.; George, M. W.; Preses, J. M.; Wishart, J. F. *Appl. Spectrosc.* **2010**, *64*, 563.

(6) (a) Schwarz, H. A. *J. Chem. Phys.* **1977**, *67*, 5525. (b) Meunier, H.; Pagsberg, P.; Sillesen, A. *Chem. Phys. Lett.* **1996**, *261*, 277.

(7) Le Caër, S.; Vigneron, G.; Renault, J. P.; Pommeret, S. *Chem. Phys. Lett.* **2006**, *426*, 71.

(8) Butler, J. M.; George, M. W.; Schoonover, J. R.; Dattelbaum, D. M.; Meyer, T. J. *Coord. Chem. Rev.* **2007**, *251*, 492.

(9) In principle, laser flash photolysis could be performed with visible light (λ > 480 nm, where the Mn complex does not absorb), using a visible-light absorbing photosensitizer in the presence of a sacrificial electron donor, resulting in intermolecular electron transfer to the Mn complex. However, in that case the chemistry may be more complex and follow a different mechanism, as has been shown in ref 3.

(10) (a) Bell, I. P.; Rodgers, M. A. J.; Burrows, H. D. *J. Chem. Soc., Faraday Trans. I* **1977**, *73*, 315. (b) Buxton, G. V.; Mulazzani, Q. G. Radiation-Chemical Techniques. In *Electron Transfer in Chemistry*; Balzani, V., Ed.; Wiley-VCH: Weinheim, Germany, 2001; Vol. *I-1*, pp 503−557. (c) Shkrob, I. A.; Sauer, M. C. *J. Phys. Chem. A* **2002**, *106*, 9120.

(11) Burrows, H. D.; Kosower, E. M. *J. Phys. Chem.* **1974**, *78*, 112.

(12) Hartl, F.; Rossenaar, B. D.; Stor, G. J.; Stufkens, D. J. *Recl. Trav. Chim. Pays-Bas* **1995**, *114*, 565.

(13) Frisch, M. J. et al. *Gaussian 09*, revision B.01; Gaussian, Inc.: Wallingford CT, 2010.

(14) The skewed *cis* isomer was chosen for the calculation since it was shown in ref 17b to be the most stable isomer of the [Re(bpy)(CO)$_3$]$_2$ dimer in THF solution.

(15) Note: weak bands seen at 1955 and 1853 cm^{-1} in the 40 ns spectrum are due to a small amount of the second transient species that has already formed at this time delay (see Figure S8).

(16) Smieja, J. M.; Kubiak, C. P. *Inorg. Chem.* **2010**, *49*, 9283.

(17) (a) Hayashi, Y.; Kita, S.; Brunschwig, B. S.; Fujita, E. *J. Am. Chem. Soc.* **2003**, *125*, 11976. (b) Fujita, E.; Muckerman, J. T. *Inorg. Chem.* **2004**, *43*, 7636.

(18) Kalyanasundaram, K. *J. Chem. Soc., Faraday Trans. 2* **1986**, *82*, 2401.

(19) (a) Klein, A.; Vogler, C.; Kaim, W. *Organometallics* **1996**, *15*, 236. (b) Stor, G. J.; Hartl, F.; Vanoutersterp, J. W. M.; Stufkens, D. J. *Organometallics* **1995**, *14*, 1115.

(20) Johnson, F. P. A.; George, M. W.; Hartl, F.; Turner, J. J. *Organometallics* **1996**, *15*, 3374.